JOURNAL OF GEOPHYSICAL RESEARCH, VOL. 113, C08028, doi:10.1029/2008JC004794, 2008

Physical and geographical origins of the South China Sea Warm Current

Tzu-Ling Chiang,[1] Chau-Ron Wu,[1] and Shenn-Yu Chao[2]

Received 1 March 2008; revised 21 May 2008; accepted 30 June 2008; published 16 August 2008.

[1] We examine the formation mechanism of the South China Sea Warm Current in winter, using a high-resolution, numerical model. The current, noted for its ability to flow against the prevailing northeast monsoon in winter, has received considerable attentions in recent years. The collective wisdom from previous models points to two likely generation scenarios: occasional wind relaxation or the Kuroshio intrusion. The present model consistently points to the wind relaxation as the dominant mechanism. When comparing differences between previous models and ours, we also conclude that the Kuroshio intrusion helps, but is not chiefly responsible. Tracing the current to the source, we identify the elevated sea level in the Gulf of Tonkin, induced by the northeast monsoon, as the ultimate driving force. The presence of Hainan Island bears little importance in generating the current.

Citation: Chiang, T.-L., C.-R. Wu, and S.-Y. Chao (2008), Physical and geographical origins of the South China Sea Warm Current, *J. Geophys. Res.*, *113*, C08028, doi:10.1029/2008JC004794.

1. Introduction

[2] Off the southeastern Asian continent, the South China Sea (SCS) is the largest marginal sea in the Pacific Ocean (Figure 1a). Waters are generally shallow (less than 60 m) in its northwestern and southwestern reaches but deepen to over 5000 m in its central and eastern basin. Consequently, the northern South China Sea (NSCS) is shallow to the northwest but deep to the east (Figure 1b). Isobaths bounding the continental slope region roughly parallel the coastline of China. Around the NSCS, the Luzon Strait is the main and only deep passage to the Pacific Ocean. In contrast, the northern passage (Taiwan Strait) to the East China Sea is quite shallow. Circulation in the NSCS is driven by the East Asian monsoons: northeasterly in winter and southwesterly in summer. The winter winds drive a basin-scale cyclonic gyre intensifying along the western boundary, and the NSCS circulation is also modified by the time-varying Kuroshio intrusion from the Luzon Strait. Both the cyclonic gyre and the Kuroshio intrusion current are mainly over the continental slope region and beyond; circulation over the shelf can be quite different.

[3] Near the northwestern shelf region, there is an alleged South China Sea Warm Current (SCSWC) flowing against the prevailing northeast monsoon in winter. Earlier studies about the SCSWC were mainly based on hydrographic data [e.g., *Guan*, 1978, 1985]. As the northeast monsoon wind prevails, the SCSWC was perceived as a strong, narrow band of northeastward current that persists all winter long. However, the monsoon wind gust may prevent it from surfacing from time to time. Its width is about 160–300 km, and the maximum surface current speed is estimated to be 0.3 m s^{-1} [*Guan*, 1978]. According to *Guan* [1978], the SCSWC is mostly confined between 200 m and 400 m isobaths based on earlier inaccurate bathymetry charts. After 30 years of improvement in bathymetry data, we have double-checked his region of interest and updated the relevant isobaths bounding the SCSWC as 100 m and 300 m isobaths. The duration of the current is about 4–6 months and the along-shore extent is roughly from 111°E to 117°E according to *Guan* [1985]. The current probably originates from the vicinity of the Hainan Island and reaches as far north as the southern part of the Taiwan Strait. The Dongsha Islands and surrounding reef may cause the SCSWC to bifurcate. The eastern branch flows steadily northeastward, while the western branch contains seasonal variations in the flow path, width, salinity and flow velocity [*Guan*, 1985; *Hsueh and Zhong*, 2004]. On the basis of a mooring observation (T1 in Figure 1b) between 5 November 2001 and 21 March 2002, *Yang* [2006] pointed out that a northeastward current off the continental shelf existed only when the northeast monsoon is weak.

[4] Previous models, numerical and analytical alike, suggested two generating mechanisms: Kuroshio intrusion or wind relaxation. *Ye* [1994] suggested that, because of the winter intrusion of the warm Kuroshio water onto the continental slope, the temperature increase from shelf to slope could geostrophically induce the SCSWC. However, the alleged SCSWC, confined between the China coastline and 100 m isobath, is far too close to shore relative to the observation-based estimate. *Chao et al.* [1995] attributed the cause to wind relaxation; the northeast monsoon piles up waters downwind and the consequent pressure gradient

[1]Department of Earth Sciences, National Taiwan Normal University, Taipei, Taiwan.
[2]Horn Point Laboratory, Center for Environmental Science, University of Maryland, Cambridge, Maryland, USA.

0148-0227/08/2008JC004794$09.00

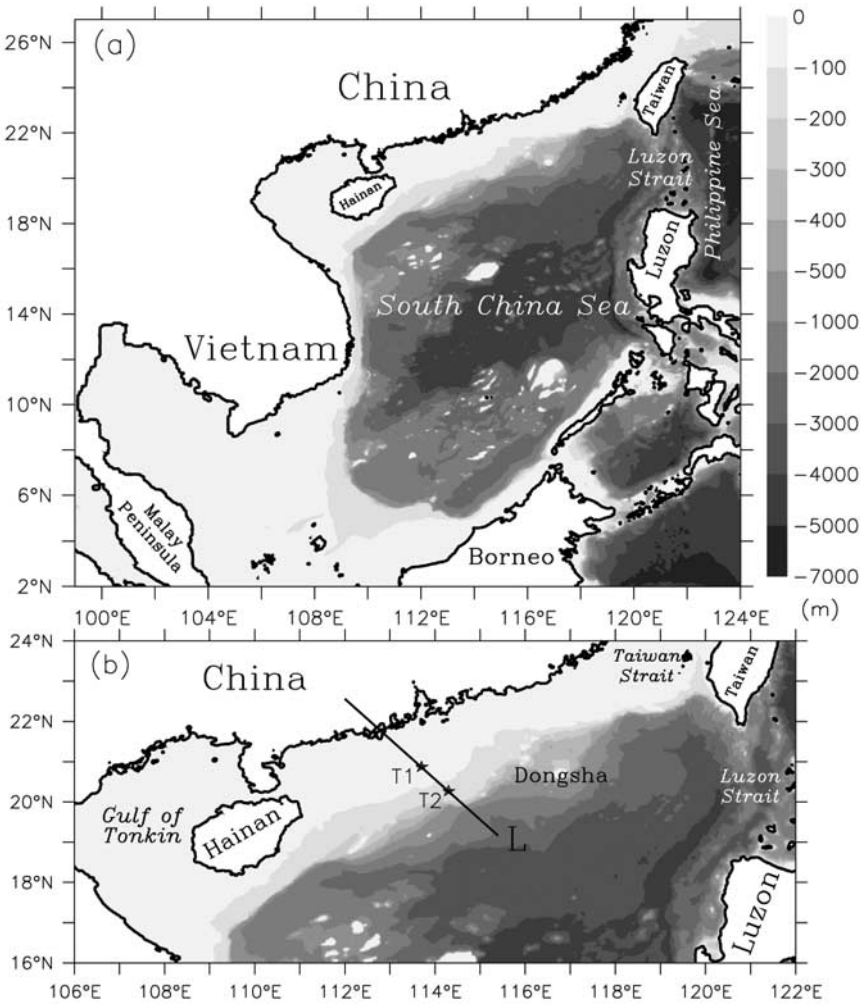

Figure 1. (a) South China Sea model domain with realistic bathymetry. (b) The topography of the northern South China Sea (NSCS) and section L that intercepts mooring station T1 and T2. Water depths are 80 m at T1 (20.86°N, 113.70°E) and 150 m at T2 (20.26°N, 114.3°E).

force drives the SCSWC after the wind relaxes. Because of the coarse model resolution (0.4°), their modeled SCSWC does not have a visible warm core. *Hsueh and Zhong* [2004] attributed it to the on-shelf impingement of the Kuroshio intrusion current into the NSCS; the consequent pressure gradient force along the shelf break induces the SCSWC as an arrested topographic wave. The axis of SCSWC in their numerical model, generally shoreward of 100 m isobath, is displaced shoreward. *Xue et al.* [2004] also attributed the SCSWC to the Kuroshio intrusion and suggested the consequent cross-shore gradients of density and sea level as the driving force. The axis of their modeled SCSWC, generally confined between 50 m and 100 m isobaths, is again too shoreward. Further, the origin of their modeled SCSWC is displayed to the northeast by more than 600 km relative to the observation-based estimate.

[5] The divergence in the school of thoughts may be a result of changing methodology over time. Limited computation power necessitated the use of coarse horizontal grids in earlier models. The lack of more realistic atmospheric forcing also necessitated the use of monthly climatological forcing, which suppresses transients. Some models did not cover the entire SCS domain. Even if they did, the imposition of open ocean boundary conditions without a larger-domain model to guide it often required a leap of faith in earlier models. Leaving technical limitations aside, the earlier models do collectively shed lights on the dominant physics leading to SCSWC. For example, *Chao et al.* [1995] almost completely eliminated the winter intrusion of Kuroshio into the SCS because of the coarse resolution; wind relaxation became the only way to produce the SCSWC. The other three models [*Ye*, 1994; *Hsueh and Zhong*, 2004; *Xue et al.*, 2004] considered the effect of the Kuroshio intrusion in the absence of wind relaxation effect; the SCSWC became too close to shore.

[6] In this work, we use a fine-resolution SCS model with much more realistic forcing and topography to investigate the SCSWC. In addition to a realistic simulation, we also conduct several thought experiments to distinguish the role of wind forcing and topographic forcing. Section 2 gives a brief description of the SCS model. Model results and

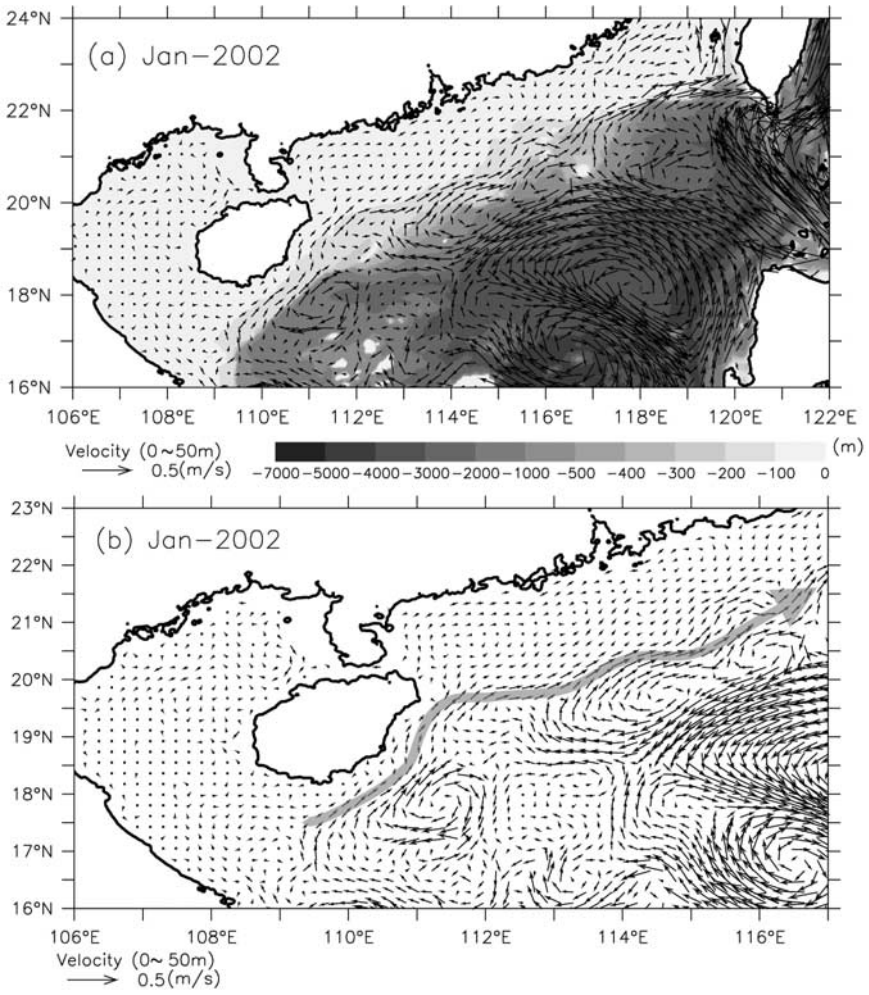

Figure 2. (a) The surface mean flow, averaged over the top 50 m, in January 2002. Shading indicates topography in the NSCS. (b) A close-up view of the South China Sea Warm Current (SCSWC) region; the broad arrow indicates the axis of the SCSWC.

thought experiments for the SCSWC are in section 3. Discussion and conclusions follow.

2. Brief Model Description

[7] The SCS model is based on the sigma coordinate Princeton Ocean Model (POM) [*Mellor*, 2004]. The three-dimensional, free surface model solves the primitive equations for momentum, salt and heat. The model domain extends from 99°E to 124°E in longitude and from 2°N to 27°N in latitude (Figure 1a). The horizontal grid size is 1/16° (about 6.8 km) and there are 26 sigma levels in the vertical. The SCS model derives its initial temperature, salinity, sea surface height (SSH) and velocity distributions from the monthly mean of a larger domain East Asian Marginal Seas (EAMS) model outputs in January 1999 [*Wu and Hsin*, 2005]. Wind forcing fields are derived from a space and time blend of QSCAT-DIRTH satellite scatterometer observations and NCEP analyses [*Milliff et al.*, 1999]. The QSCAT/NCEP blended wind product has a time interval of 6 h and a spatial resolution of 0.5° × 0.5°. The model is subject to wind stress at the sea surface and forcing on open ocean boundaries provided by the EAMS model, which is also driven by the QSCAT/NCEP blended wind forcing. The simulation period is from 1999 to 2005.

[8] A detailed description of the SCS model has been given by *Wu and Chiang* [2007]. The model has been well validated by the observed temperature from a time series station as well as current velocity data from several mooring stations in the SCS, including station T1 [*Wu and Chiang*, 2007]. In particular, the correlation between mooring data and modeled velocity at station T1 from 5 November 2001 to 31 March 2002 reaches 0.7 with no time lag [*Yang*, 2006]. Further, the annual modeled mean transport from the Luzon Strait is about 2.8 Sv, comparable to the observation-based estimate of 3 Sv [*Qu*, 2000].

3. Results

3.1. Flow Pattern and Vertical Structure of the SCSWC

[9] Figure 2a shows the simulated monthly mean (January 2002) surface flow, averaged over the top 50 m, in the region of interest. In it, the largest westward component of the Kuroshio intrusion is through the deepest channels of the Luzon Strait (the Balintany Channel at about 122°E and

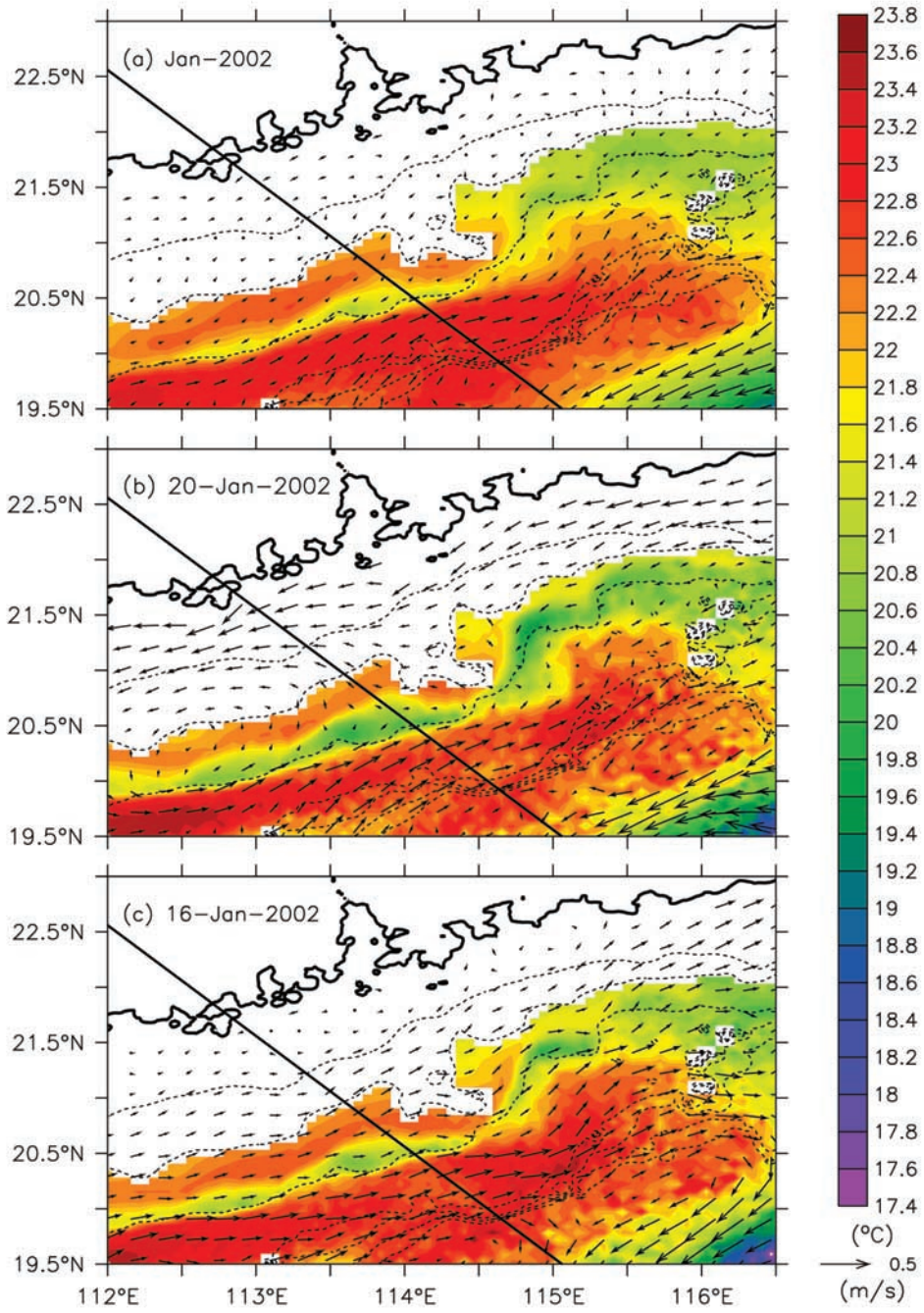

Figure 3. The surface flow pattern, averaged over the top 50 m, and temperature at 75 m depth (a) in January 2002, (b) on 20 January 2002, and (c) on 16 January 2002. Isobath contours are 50, 75, 100, 200, 300, 400, and 500 m. The thick black line indicates transect L in Figure 1b.

19.5–20.4°N) and the largest outflow (eastward) is through the Bashi Channel between southern Taiwan and Batan Island (at about 122°E and 20.8°N). These features agree with previous findings from both drifter data [*Centurioni et al.*, 2004, Figure 5] and composite shipboard acoustic Doppler current profiler (ADCP) data [*Liang et al.*, 2003, Figure 12]. Furthermore, the SCSWC stands out as a continuous current mainly bounded by 100 m and 300 m isobaths (Figure 2b). It originates from about 109°E or south of the Hainan Island. The maximum velocity is about 0.3 m s^{-1} near 114°E, 20°N, which is in a good agreement with the estimate based on hydrographic data [*Guan*, 1978].

[10] Zooming in, Figure 3a shows the same mean surface flow (0–50 m) for January 2002, superimposed on temperature field at 75 m depth, while Figures 3b and 3c show corresponding daily averages on 20th and 16th of the month, respectively. The northeast monsoon is large scale in nature. In consequence, the wind intensity and direction

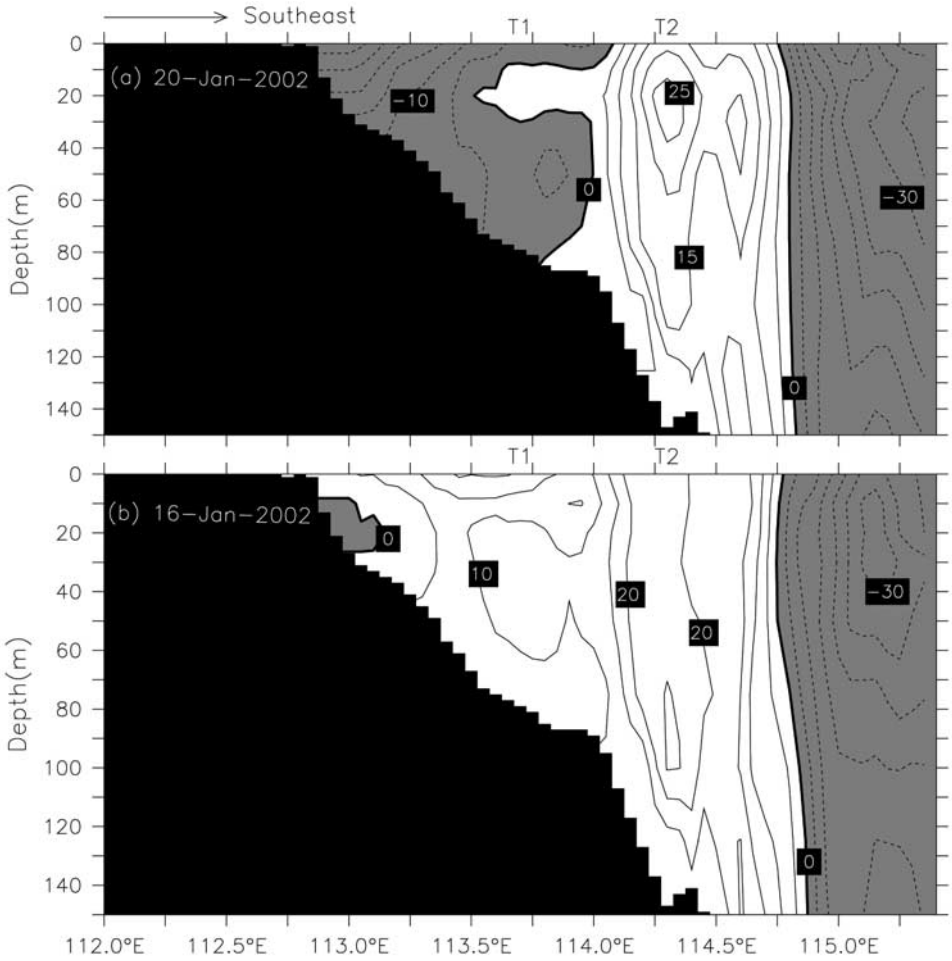

Figure 4. Along-shore velocity profiles along section L on (a) 20 January 2002 and (b) 16 January 2002. The contour interval is 5 cm s^{-1}. Solid and dashed thin lines indicate northeastward and southwestward currents, respectively. Shading indicates negative contours.

do not change appreciably over the entire region of the NSCS. In this month of interest, the wind forcing is the strongest on the 20th and weakest on the 16th. We use these two snapshots for illustrative purpose only. The conclusions below also hold at other times as well. In Figures 3a, 3b, and 3c, the narrow band of higher temperature, bounded between 100 m and 300 m isobaths, harbors the SCSWC that carries warm waters from the southwest to the northeast. The persistence of SCSWC in the monthly average (Figure 3a) indicates its presence most of the time in January of 2002. Furthermore, whether the wind stress is the strongest (Figure 3b) or weakest (Figure 3c), the northeastward SCSWC always exists near the shelf break region between 100 and 300 m isobaths in this period. On the other hand, downwind acceleration is much more evident in shallower shelf region (less than 100 m). Unlike the steadily northeastward current near the shelf break, the current in the shallower region flows to the southwest (northeast) as the northeast monsoon wind becomes stronger (weaker).

[11] Cross section L of the SCSWC in Figure 1b intercepts mooring station T1 and T2. Prior model validation with those ADCP mooring data [*Wu and Chiang*, 2007] enables us to address the vertical structure of SCSWC with reasonable confidence. Following this cross section, Figure 4 illustrates markedly different responses to wind forcing near stations T1 and T2; the latter is far less intuitive than the former. The SCSWC is located between 114–114.6°E and station T2 is near its core. The maximal core speed is around 0.3 m s^{-1} (northeastward) when the adverse wind is the strongest (Figure 4a), but decreases to 0.25 m s^{-1} when the wind is weaker (Figure 4b). The intensification against strengthened wind is counterintuitive. Even more so, the core depth is about 25 m when the adverse wind is the strongest, but descends to about 70 m when the wind is weaker. Thus, the baroclinic aspect of the wind-driven response is far from being local and far more complex than a linear superposition.

[12] Over the shallower shelf, the wind-driven response near station T1 is more intuitive. Currents generally flow southwestward (downwind) under stronger wind condition (Figure 4a). As the northeasterly winds relax, the shelf current becomes northeastward, in the same direction of the SCSWC (Figure 4b).

[13] Another point is also noteworthy. Under both strong and weak wind conditions, the SCSWC in Figure 4 persistently shows vertical coherence down to 150 m depth, suggesting the relative unimportance of the wind-driven

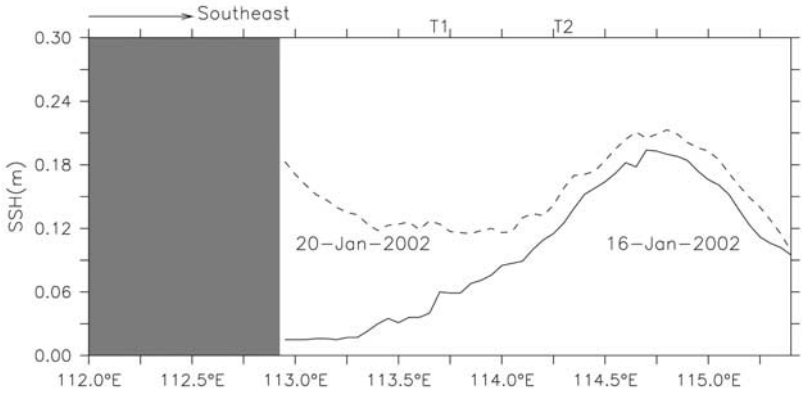

Figure 5. Sea surface height (SSH) along section L on 20 January 2002 (dashed line) and 16 January 2002 (solid line). Gray shading indicates the land.

Ekman effect in maintaining the current. The momentum balance, to be illustrated in Figure 6, also supports this conclusion.

3.2. Formation Mechanism of the SCSWC

[14] During the model simulation period, the winter SCSWC is not always persistent, but takes place from time to time. The variations of wind stress and bathymetry may influence its duration. The modeled SCSWC persists stably from November 2001 to March 2002; we choose this period to facilitate the analysis below.

[15] Figure 5 shows the SSH along section L on 16 and 20 January 2002. Eastward of 114°E, the SSH first rises to maximum near 114.6°E and decreases thereafter. This is true whether the northeast monsoon is the weakest (on the 16th) or strongest (on the 20th). Westward of 114°E, SSH generally continues to decrease shoreward if the wind is the weakest (on the 16th), but rises shoreward if the wind is the strongest (on the 20th). If geostropy prevails, there appears to be two forces working against each other in the SCSWC region and shoreward. The wind forcing tends to drive current downwind and a remote force tends to drive the current against the wind. In shallow reaches west of 114°E, the former can overcome the latter under strong wind conditions. In the SCSWC region east of 114°E, the latter usually prevails in this period. Both *Chao et al.* [1995] and *Hsueh and Zhong* [2004] suggested the along-shore sea level gradient as the remote force driving the SCSWC, even though their opinions differ in the origin of the sea level gradient (the former attributed it to wind relaxation while the latter, to the on-shelf intrusion of the Kuroshio Current.)

[16] We examine the importance of sea level gradients at station T2 below. Sea level gradients appear explicitly in vertically averaged momentum equations for along-shore (u_0) and cross-shore (v_0) velocities. In linear forms, they are

$$\frac{\partial u_0}{\partial t} - fv_0 = -\frac{1}{\rho}\frac{\partial P}{\partial x} + \frac{\tau_x}{\rho H} - \mathrm{F}_x$$
$$\frac{\partial v_0}{\partial t} + f\mathrm{u}_0 = -\frac{1}{\rho}\frac{\partial P}{\partial \mathrm{y}} + \frac{\tau_\mathrm{y}}{\rho H} - \mathrm{F}_\mathrm{y}$$

where f is Coriolis parameter, ρ is water density, P is pressure, τ is wind stress, H is the local depth, and F represents friction. Figures 6a and 6b compare the relative importance of current acceleration, Coriolis force, pressure gradient force and wind stress in the cross-shore and along-shore direction, respectively. To let the conclusion stand out, we also superimpose corresponding cross-shore and along-shore velocities, averaged over the top 50 m, in Figures 6a and 6b, respectively. In the cross-shore direction (Figure 6a), one sees reasonable correlation between surface current (black line) and Coriolis force (blue line). In terms of instantaneous momentum balance, the Coriolis force induced by the along-shore current is balanced by the cross-shore pressure gradient (red line). Thus, the cross-shelf balance is approximately geostrophic. In the along-shore direction (Figure 6b), the surface current (black line) correlates reasonably well with pressure gradient force (red line). In particular, the SCSWC appears whenever the sea level gradient force is positive (northeastward), pointing out the predominance of along-shore sea level gradient force in driving the SCSWC. In either the cross-shelf or along-shelf balance, the wind stress effect (green line in Figure 6) appears to be negligible, indicating the unimportance of wind-driven Ekman transport in maintaining the SCSWC. Further, the northeastward pressure gradient force contains a strong barotropic component when the SCSWC appears and therefore does not intensify in the thermocline layer.

[17] We also found that the northeastward pressure gradient force takes place only when northeast wind relaxes. Figures 7a and 7b compare the modeled along-shore velocity, averaged over the top 50 m, with the along-shore wind stress at stations T1 and T2 from December 2001 to February 2002. The best linear regression fit at T1 leads to

$$u\left(\mathrm{m\ s^{-1}}\right) = 0.66 \times \tau_\mathrm{y}\left(\mathrm{N\ m^{-2}}\right) + 0.10$$

with a regression coefficient (γ) of 0.71. The corresponding fit at T2 is

$$u\left(\mathrm{m\ s^{-1}}\right) = 0.66 \times \tau_\mathrm{y}\left(\mathrm{N\ m^{-2}}\right) + 0.24$$

with a regression coefficient of 0.64. Rather amazingly, both lines have the same slope, suggesting identical response to wind forcing. The u intercept is 0.10 m s^{-1} at station T1 and

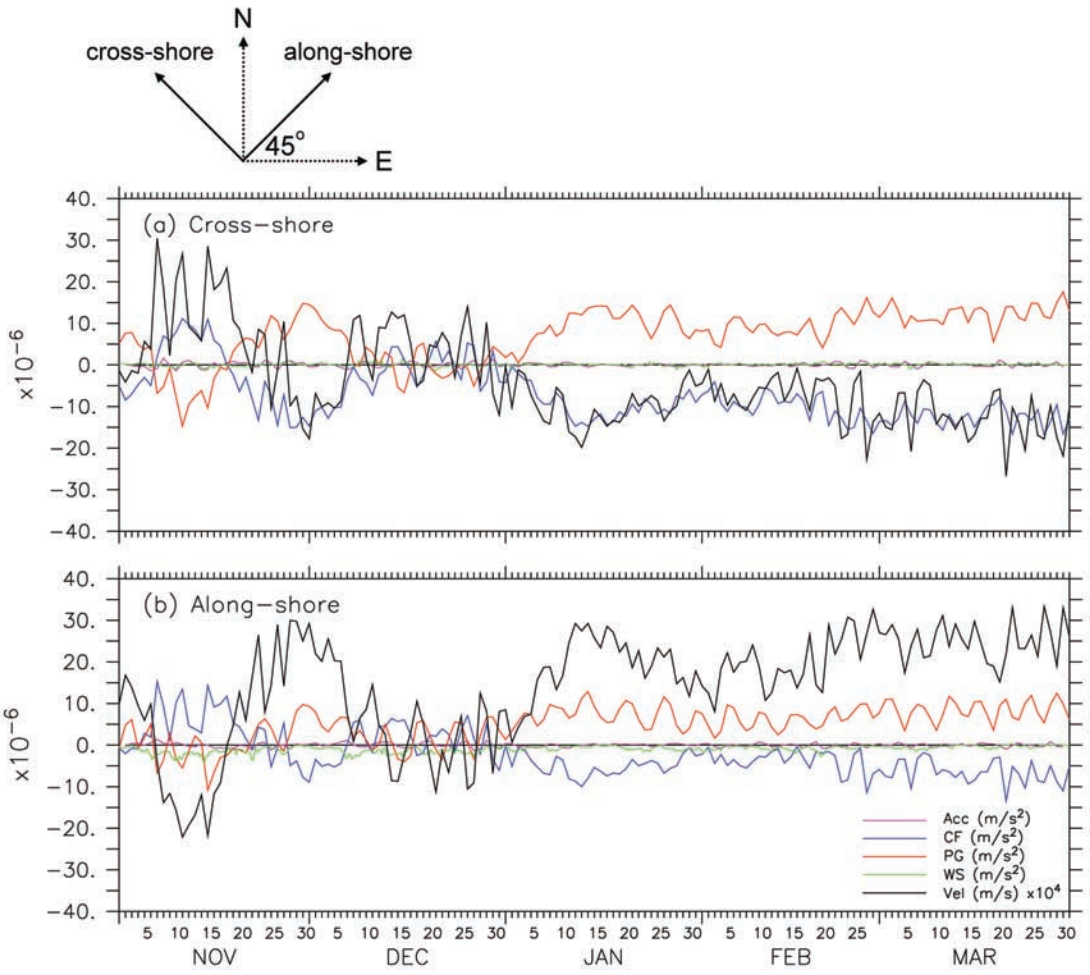

Figure 6. Velocity averaged over top 50 m (black), acceleration (magenta), Coriolis force (blue), pressure gradient (red), and wind stress (green) at station T2. Time series in (a) cross-shore direction and (b) along-shore direction are from November 2001 to March 2002.

0.24 m s^{-1} at station T2, indicating a stronger northeastward flow near T2 (the core of SCSWC) if the wind stress decreases to zero. With a typical wind stress of 0.15 N m^{-2} in winter, the current practically disappears at station T1 but still maintains a viable speed of 0.14 m s^{-1} northeastward at station T2. For convenience, we use 0.14 m s^{-1} hereafter as a benchmark to measure the survivability of winter SCSWC near station T2.

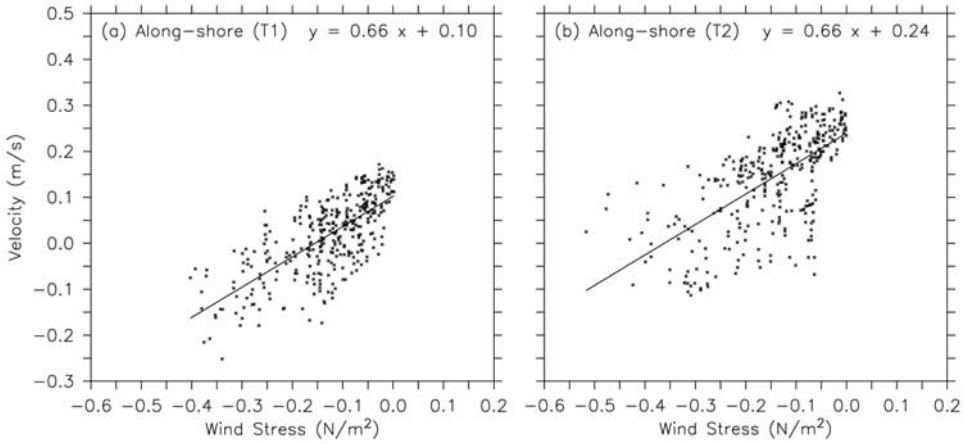

Figure 7. Regressions of along-shore wind stress and along-shore velocity averaged over the top 50 m at stations (a) T1 and (b) T2.

Table 1. List of Wind Forcing Thought Experiments

	Case	Constant Wind Stress (N m^{-2})		
Experiment set 1	1a	0		
	1b	0.1 (NE)		
	1c	0.2 (NE)		
	1d	0.4 (NE)		
		Initial Wind Stress (N m^{-2})		
	Deceleration Rate (% d^{-1})	0.1 (NE)	0.2 (NE)	0.4 (NE)
Experiment set 2	100	Case 2a	Case 2e	Case 2i
	50	Case 2b	Case 2f	Case 2j
	25	Case 2c	Case 2g	Case 2k
	12.5	Case 2d	Case 2h	Case 2l
	Case	Acceleration Rate of NE Wind Stress (N m^{-2} d^{-1})		
Experiment set 3	3a	0.05		
	3b	0.1		
	3c	0.2		
	3d	0.4		

3.3. Thought Experiments About Wind Forcing

[18] The northeast monsoon may drive the northeastward pressure gradient force, which in turn drives the northeastward SCSWC. To examine the sensitivity of SCSWC to wind intensity and wind fluctuation, we conduct three sets of thought experiments by deviating slightly from the realistic simulation. Table 1 summarizes the experiments to be discussed below.

3.3.1. Experiment Set 1: Constant Wind Forcing

[19] We restart the model from 1 January 2002 by applying a constant, northeasterly wind stress of 0, 0.1, 0.2 or 0.4 N m^{-2}; on this day the realistic wind stress was about 0.07 N m^{-2} and the northeastward current was too weak (0.08 m s^{-1}) to be identified as SCSWC. Figure 8 shows the along-shore velocity at T2, averaged over the top 50 m, for the first 7 days. The abrupt application of constant wind forcing invariably triggers some fluctuations related to propagation of transient Rossby and coastal waves. Leaving these fluctuations aside, the current in all cases first decelerates or even reverses before rebounding. Under the no-wind condition (Case 1a), a sizable SCSWC emerges after 1.5 days because of wind relaxation. Further strengthening of the wind stress eliminates the possibility of SCSWC altogether. In the extreme, the 0.4 N m^{-2} wind stress in Case 1d reverses the current completely. In conclusion, the SCSWC may come into existence only under weaker wind conditions.

3.3.2. Experiment Set 2: Wind Deceleration

[20] The weakening rate of wind stress also affects the formation of SCSWC. Starting again from 1 January 2002, the initial wind stress is set to be 0.1, 0.2, and 0.4 N m^{-2}, respectively. After spinning up for the first day, we decrease wind forcing linearly to zero in 1, 2, 4 or 8 days. Corresponding decreasing rates are 100%, 50%, 25% or 12.5% per day. Leaving oscillations aside, all cases lead to the emergence of northeastward SCSWC in time (Figure 9). Both the deceleration rate and initial intensity of wind forcing influence the timing of SCSWC appearance. With the same initial wind intensity, a slower deceleration would delay the onset of SCSWC. If the initial wind intensity is stronger, the delay is more profound given the same deceleration rate.

3.3.3. Experiment Set 3: Wind Acceleration

[21] We pick the beginning of the fifth day from Case 2i (Figure 9c) as the initial day, when the SCSWC is already established and the wind stress is about zero, to restart the model. Thereafter the acceleration rate for the northeast wind stress is 0.05, 0.1, 0.2 or 0.4 N m^{-2} per day. As expected, faster wind acceleration leads to faster disappearance of SCSWC (Figure 10). Transporting this result to reality, winter passages of fronts should greatly affect the survivability of SCSWC, and sudden onset of a strong blast may cut off the SCSWC completely in 1 day.

4. Discussion

[22] The buildup of sea level gradient by the northeasterly monsoon forms the along-shore pressure gradient forcing,

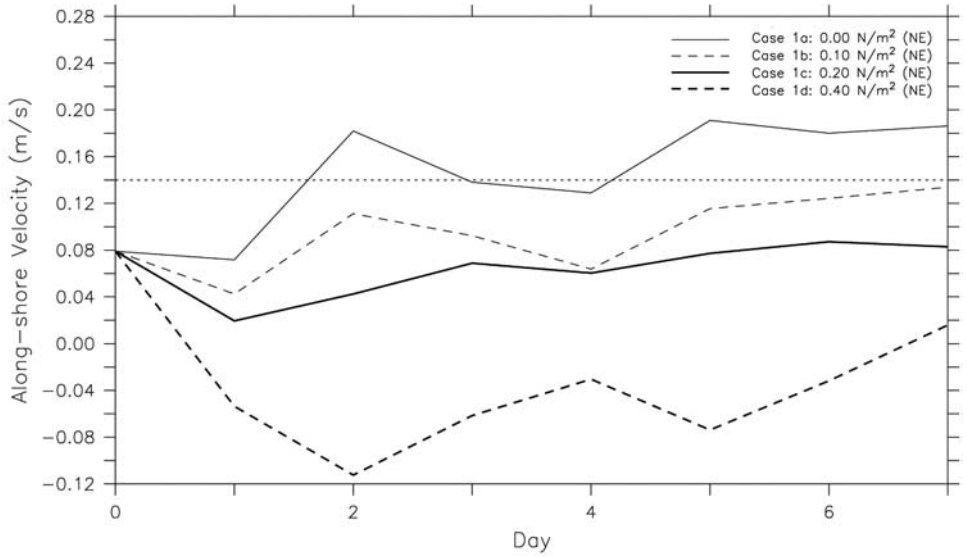

Figure 8. Surface mean flows averaged over the top 50 m at station T2 in Cases 1a–1d.

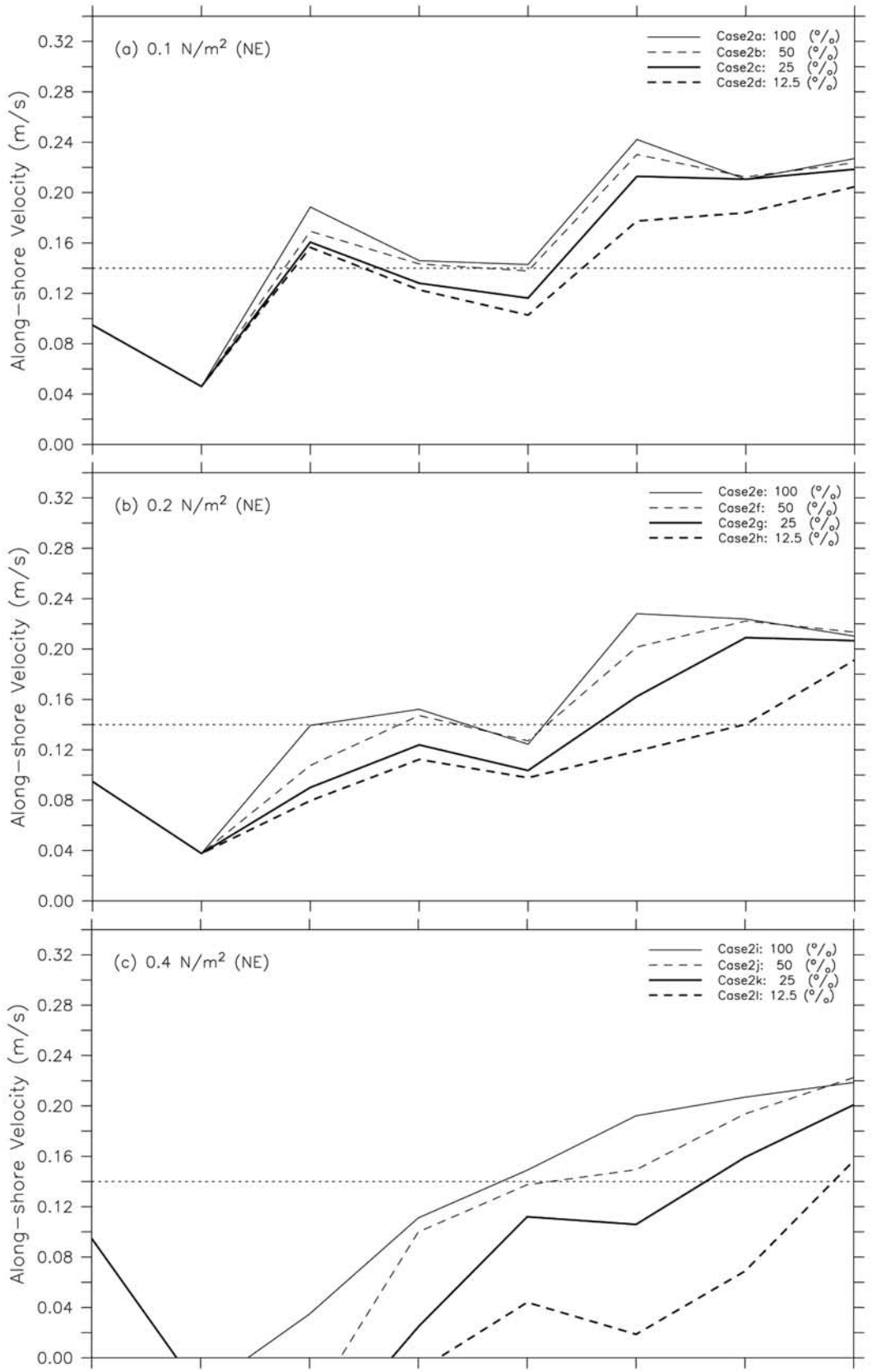

Figure 9. Surface mean flows averaged over the top 50 m at station T2 in (a) Cases 2a–2d, (b) Cases 2e–2h, and (c) Cases 2i–2l.

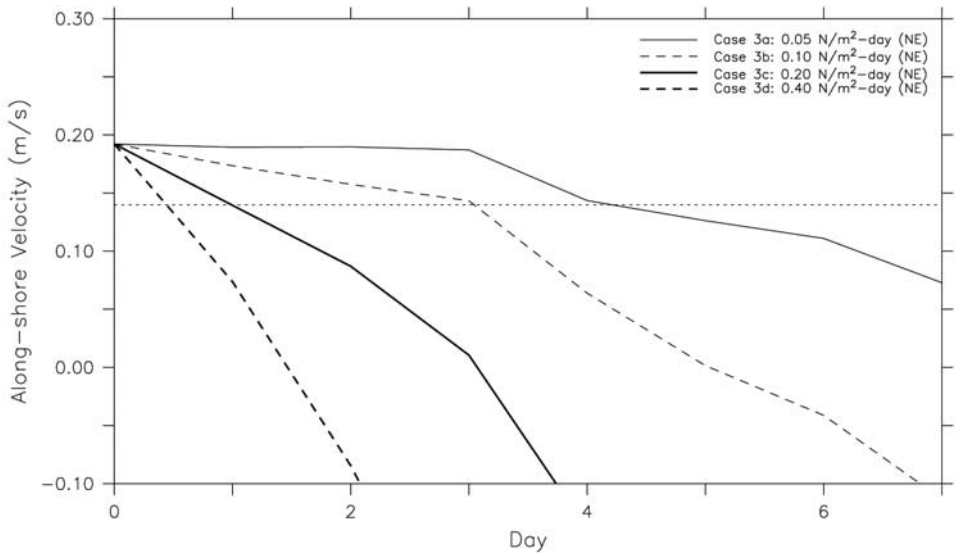

Figure 10. Surface mean flows averaged over the top 50 m at station T2 in Cases 3a–3d.

which, when combined with weakened northeast monsoon, will trigger the northeastward SCSWC. *Guan* [1985] suggested the region southeast off Hainan Island as the origin of SCSWC. In his argument, the Hainan Island is essentially a solid wall for water buildup. To investigate this possibility, Figure 11 shows modeled surface flow and SSH, with and without the Hainan Island, in January 2002. In conclusion, the present model does not support the speculation. The January mean with the Hainan Island (Figure 11a) shows the persistence of elevated sea level in the Gulf of Tonkin;

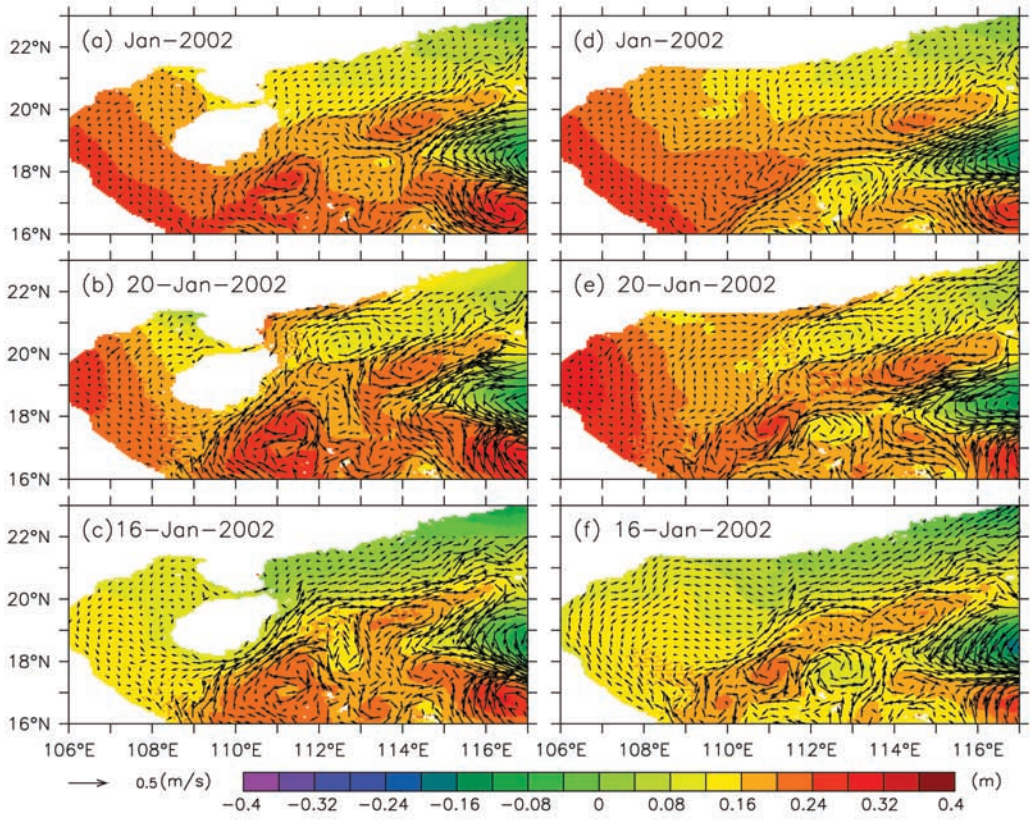

Figure 11. Surface mean flow patterns averaged over the top 50 m and SSH with the Hainan Island (a) in January 2002, (b) on 20 January 2002, and (c) on 16 January 2002. (d, e, and f) Corresponding model results after removing the Hainan Island.

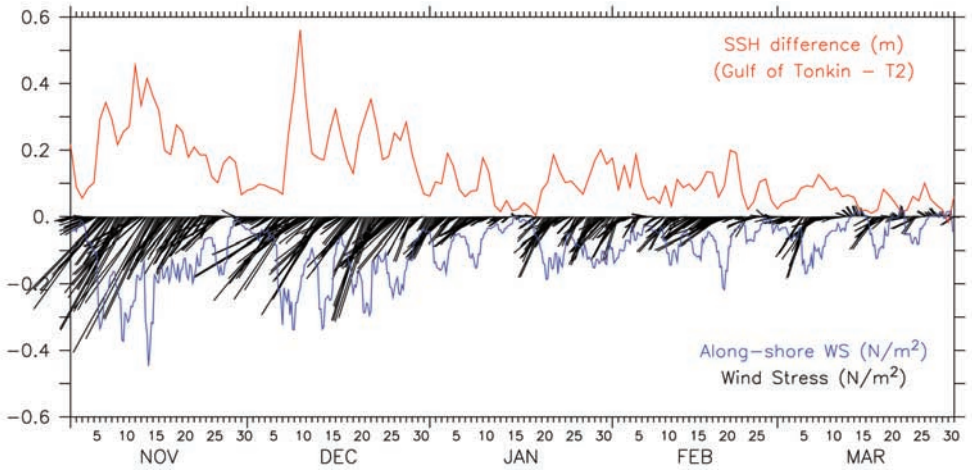

Figure 12. Wind stress over the NSCS (black), along-shore wind stress over the NSCS (blue), and Gulf of Tokin SSH elevation over T2 station (red) from November 2001 to March 2002. The Gulf of Tokin domain extends from 106°E to 107°E and from 17°N to 18°N.

the Hainan Island is apparently unable to block the buildup. On 20 January, when the northeast monsoon was the strongest of the month, the sea level buildup is pushed to the westernmost reaches of the Gulf (Figure 11b). On 16 January, when the northeast monsoon was the weakest of the month, the elevated sea level in the Gulf is unleashed somewhat, but still higher than that along the main path of the SCSWC (Figure 11c). In other words, the sea level is always elevated in the Gulf of Tonkin regardless of wind intensity, suggesting that Hainan Island may not be an efficient blocker. To be certain, Figures 11d, 11e, and 11f show corresponding results with the Hainan Island removed. The water still piles up around the southwestern Gulf of Tonkin as before. With or without the Hainan Island, the highest SSH is always to west of it, indicating the inability of the Island to block incoming waters. The SSH in the Gulf of Tonkin is also highly correlated with the wind stress. In particular, the average wind stress over the NSCS and SSH in the piling region have a large and negative correlation (−0.87); the former leads the latter by 1 day.

[23] Figure 11 also shows that the SCSWC does not owe its existence to the Hainan Island. Removing the island only weakens the SCSWC slightly. The source location of SCSWC is not very sensitive to the existence of Hainan Island either. The SCSWC can be traced back to the vicinity of 16.5°N and 109°E. When wind relaxes, waters exiting the Gulf of Tonkin from the source region enter deep water abruptly. Potential vorticity constraint would require the outflow to gain positive vorticity, or to turn cyclonically, forming the beginning of SCSWC.

[24] A sea level index would help bringing the foregoing results to focus. We average the modeled SSH over the Gulf of Tonkin and subtract SSH at station T2 from it. Figure 12 shows the resulting sea level difference (red), sampled at daily intervals from November 2001 to March 2002. Also shown is the corresponding 6 hourly wind stress (black sticks) and along-shore wind stress (blue) averaged over the NSCS. The sea level index is always positive in the entire winter. Wind modulations on event-like timescales are apparent. When the northeast monsoon is strong, SSH over the Gulf of Tonkin elevates significantly relative to that at station T2. Occasional wind relaxations (for example, from 26 to 30 November 2001 and from 10 to 16 January 2002) decrease the sea level index markedly. Modulations on seasonal timescales are also apparent. From December to March, for example, the wind intensity generally decreases in time, so does the sea level index.

[25] To further accentuate the importance of wind relaxation over Kuroshio intrusion, we have also closed the eastern boundary of the model domain (at 124°E in Figure 1a) from 1 January 2001 to 31 January 2002 to eliminate the Kuroshio intrusion. The SCSWC survived rather well after more than 1 year of the eastern boundary closing. Figure 13a shows the resulting circulation on 16 January 2002, averaged over the top 50 m. Figure 13b shows corresponding circulation without closing the eastern boundary. West of 114°E, closing the eastern boundary makes the SCSWC slightly weaker. Around 116°E, the closing-induced weakening SCSWC is more visible. East of 118°E, the closing of the eastern boundary actually strengthens the SCSWC because of the existence of an anticyclonic eddy off the shelf. Thus, wind relaxation is more important than the Kuroshio intrusion in maintaining the SCSWC.

5. Conclusions

[26] Going back to hypotheses from previous models, does the winter SCSWC originate from the Kuroshio intrusion or wind relaxation? If it is due to Kuroshio intrusion, are cross-shore or along-shore gradients responsible? The second question is easier to answer. If the cross-shelf gradient is solely responsible, it will not be able to extend to the far west where the Kuroshio intrusion effect diminishes. The extension to the west (or upstream) of the northeastward current requires, as *Hsueh and Zhong* [2004] pointed out, an alongshore pressure gradient to trigger the arrested topographic waves.

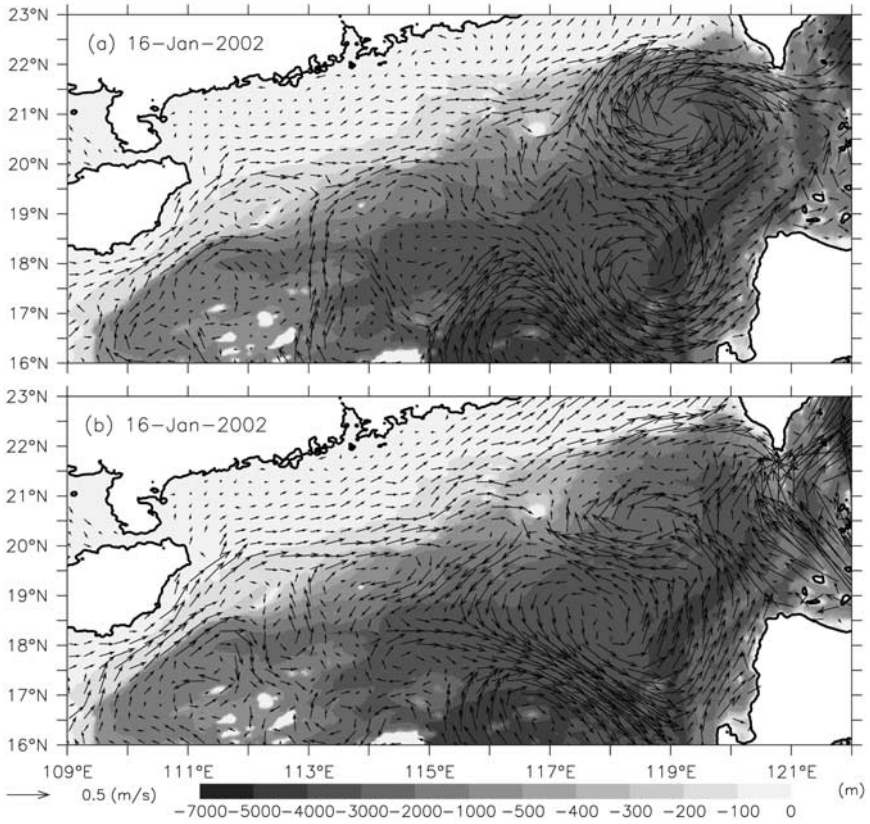

Figure 13. Surface circulation on 16 January 2002 superimposed on bottom topography. Eastern ocean boundary at 124° is shown (a) closed and (b) open.

[27] The first question requires more explanations to answer. Previous models use monthly climatological forcing, which suppresses transients. As such, the SSH buildup in the Gulf of Tonkin is not as strong and abrupt as in Figure 11; even an abrupt termination of northeast monsoon can only trigger a weak SCSWC [*Chao et al.*, 1995]. Understandably, the suppression of SSH buildup in the Gulf of Tonkin by climatology forcing allows the effect of Kuroshio intrusion to stand out better in earlier models. This is particularly true in the paper by *Hsueh and Zhong* [2004], which truncated the Gulf and Tonkin and therefore largely removed the SSH buildup in the source region. In this limit, the Kuroshio intrusion is able to generate a northeastward flow, but the current is too close to shore [*Ye*, 1994; *Hsueh and Zhong*, 2004] or additionally originates too far east [*Xue et al.*, 2004]. Our model consistently identifies the SSH buildup in the Gulf of Tonkin by the northeast monsoon as the source of winter SCSWC (Figure 12); subsequent wind relaxation produces a SCSWC that has the appropriate strength, location and origin. Further, the modeled SCSWC can survive rather well even if we terminate the winter Kuroshio intrusion (Figure 13). In conclusion, the winter SCSWC is primarily produced by wind relaxation. The Kuroshio intrusion helps, but is not chiefly responsible.

[28] **Acknowledgments.** The authors would like to thank the two anonymous reviewers for their careful review of this paper and detailed suggestions to improve the manuscript. Author C. R. W. was supported by the National Science Council, Taiwan, ROC, under grants NSC 95-2611-M-003-001-MY3 and NSC 96-2621-Z-110-002. Author S. Y. C. was supported by U. S. Office of Naval Research, Code 322 PO under contract N00014-05-1-0279. This is UMCES contribution 4203.

References

Centurioni, L. R., P. P. Niiler, and D.-K. Lee (2004), Observations of inflow of Philippine Sea water into the South China Sea through the Luzon Strait, *J. Phys. Oceanogr.*, *34*, 113–121, doi:10.1175/1520-0485(2004)034<0113:OOIOPS>2.0.CO;2.

Chao, S.-Y., P.-T. Shaw, and J. Wang (1995), Wind relaxation as a possible cause of the South China Sea Warm Current, *J. Oceanogr.*, *51*, 111–132, doi:10.1007/BF02235940.

Guan, B. (1978), The warm current in the South China Sea — A current flowing against the wind in winter in the open sea off Guangdong province (in Chinese with English abstract), *Oceanol. Limnol. Sin.*, *9*(2), 117–127.

Guan, B. (1985), Some features of the temporal and spatial distributions of the "counter-wind" current in northern South China Sea in winter (in Chinese with English abstract), *Oceanol. Limnol. Sin.*, *16*(6), 429–438.

Hsueh, Y., and L. Zhong (2004), A pressure-driven South China Sea Warm Current, *J. Geophys. Res.*, *109*, C09014, doi:10.1029/2004JC002374.

Liang, W.-D., T. Y. Tang, Y. J. Yang, M. T. Ko, and W.-S. Chuang (2003), Upper-ocean currents around Taiwan, *Deep Sea Res., Part II*, *50*, 1085–1105, doi:10.1016/S0967-0645(03)00011-0.

Mellor, G. L. (2004), Users guide for a three-dimensional, primitive equation, numerical ocean model, manual, 56 pp., Program in Atmos. and Oceanic Sci., Princeton Univ., Princeton, N. J.

Milliff, R. F., W. G. Large, J. Morzel, G. Danabasoglu, and T. M. Chin (1999), Ocean general circulation model sensitivity to forcing from scatterometer winds, *J. Geophys. Res.*, *104*(C5), 11,337–11,358, doi:10.1029/1998JC900045.

Qu, T. (2000), Upper-layer circulation in the South China Sea, *J. Phys. Oceanogr.*, *30*, 1450–1460, doi:10.1175/1520-0485(2000)030<1450:ULCITS>2.0.CO;2.

Wu, C.-R., and T.-L. Chiang (2007), Mesoscale eddies in the northern South China Sea, *Deep Sea Res., Part II*, *54*, 1575–1588, doi:10.1016/j.dsr2.2007.05.008.

Wu, C.-R., and Y.-C. Hsin (2005), Volume transport through the Taiwan Strait: A numerical study, *Terr. Atmos. Oceanic Sci.*, *16*(2), 377–391.

Xue, H., F. Chai, N. Pettigrew, D. Xu, M. Shi, and J. Xu (2004), Kuroshio intrusion and the circulation in the South China Sea, *J. Geophys. Res.*, *109*, C02017, doi:10.1029/2002JC001724.

Yang, K.-C. (2006), The non-persistent South China Sea Warm Current, M. S. dissertation, 48 pp., National Taiwan Univ., Taipei.

Ye, L. (1994), On the mechanism of South China Sea warm Current and Kuroshio Branch in winter — Preliminary result of 3-D baroclinic experiments, *Terr. Atmos. Oceanic Sci.*, *5*(4), 597–610.

S.-Y. Chao, Horn Point Laboratory, Center for Environmental Science, University of Maryland, Cambridge, MD 21613-0775, USA.

T.-L. Chiang and C.-R. Wu, Department of Earth Sciences, National Taiwan Normal University, Number 88, Section 4 Ting-Chou Road, Taipei 11677, Taiwan. (cwu@ntnu.edu.tw)